Generation of Isogenic Pluripotent Stem Cells Differing Exclusively at Two Early Onset Parkinson Point Mutations

Cell

Resource

Generation of Isogenic Pluripotent Stem Cells Differing Exclusively at Two Early Onset Parkinson Point Mutations

Frank Soldner,[1] Josée Laganière,[4] Albert W. Cheng,[1,3] Dirk Hockemeyer,[1] Qing Gao,[1] Raaji Alagappan,[1] Vikram Khurana,[1,5] Lawrence I. Golbe,[7] Richard H. Myers,[6] Susan Lindquist,[1,2] Lei Zhang,[4] Dmitry Guschin,[4] Lauren K. Fong,[4] B. Joseph Vu,[4] Xiangdong Meng,[4] Fyodor D. Urnov,[4] Edward J. Rebar,[4] Philip D. Gregory,[4] H. Steve Zhang,[4] and Rudolf Jaenisch[1,2,*]

[1]The Whitehead Institute, 9 Cambridge Center, Cambridge, MA 02142, USA
[2]Department of Biology, Massachusetts Institute of Technology, 31 Ames Street, Cambridge, MA 02139, USA
[3]Computational and Systems Biology Program, Massachusetts Institute of Technology, Cambridge, MA 02139, USA
[4]Sangamo BioSciences, Inc., Pt. Richmond Tech Center, 501 Canal Boulevard, Suite A100, Richmond, CA 94804, USA
[5]Departments of Neurology, Brigham and Women's and Massachusetts General Hospitals, Harvard Medical School, Boston, MA 02115, USA
[6]Department of Neurology, Boston University School of Medicine, Boston, MA 02118, USA
[7]Department of Neurology, UMDNJ-Robert Wood Johnson Medical School, New Brunswick, NJ 08903, USA
*Correspondence: jaenisch@wi.mit.edu
DOI 10.1016/j.cell.2011.06.019

SUMMARY

Patient-specific induced pluripotent stem cells (iPSCs) derived from somatic cells provide a unique tool for the study of human disease, as well as a promising source for cell replacement therapies. One crucial limitation has been the inability to perform experiments under genetically defined conditions. This is particularly relevant for late age onset disorders in which in vitro phenotypes are predicted to be subtle and susceptible to significant effects of genetic background variations. By combining zinc finger nuclease (ZFN)-mediated genome editing and iPSC technology, we provide a generally applicable solution to this problem, generating sets of isogenic disease and control human pluripotent stem cells that differ exclusively at either of two susceptibility variants for Parkinson's disease by modifying the underlying point mutations in the α-synuclein gene. The robust capability to genetically correct disease-causing point mutations in patient-derived hiPSCs represents significant progress for basic biomedical research and an advance toward hiPSC-based cell replacement therapies.

INTRODUCTION

Extraordinary excitement over progress in the ability of genomic medicine to connect specific genotypes to disease predisposition has been tempered by the host of challenges in translating such correlations to specific treatments. There is consensus in the field that modeling "diseases in a dish" is one of the most promising approaches to address this crucial problem (Vogel, 2010). Human induced pluripotent stem cell (hiPSC) technology, which enables the epigenetic reprogramming of human somatic cells into an embryonic stem cell-like state followed by differentiation into any cell type of the body, is being developed as a key component of such in vitro disease modeling (Dimos et al., 2008; Park et al., 2008; Soldner et al., 2009; Takahashi et al., 2007; Yu et al., 2007). In principle, patient-specific iPSCs that carry all disease-relevant genetic alterations could provide researchers with a unique opportunity to study the cellular and molecular mechanisms of monogenic and complex diseases in relevant cell types in vitro with the potential to identify alternative treatments (Daley and Scadden, 2008; Saha and Jaenisch, 2009).

However, so far, only a few such studies have identified disease-related phenotypes, mostly in rare, early age onset or metabolic diseases (Brennand et al., 2011; Ebert et al., 2009; Itzhaki et al., 2011; Lee et al., 2009; Marchetto et al., 2010; Rashid et al., 2010). Due to the robust and rapid manifestation of these disorders, in vitro models are more likely to display clear differences when compared to healthy donor controls. In contrast, late age onset disorders, such as Parkinson's and Alzheimer's diseases, with long latency and slow progression of cellular and pathological changes in vivo are expected to show only subtle phenotypes in vitro. To distinguish these subtle but disease-relevant phenotypical changes from unpredictable background-related variations could prove difficult due to the lack of genetically matched controls. Commonly used control cells from healthy donors represent an approximate solution at best because individual hESC and hiPSC lines display highly variable biological characteristics such as the propensity to differentiate into specific functional cells (Bock et al., 2011; Boulting et al., 2011; Soldner et al., 2009). The basis for these profound differences is manifold and includes: (1) differences in genetic background; (2) the process of cell derivation (Lengner et al., 2010); and (3) in the case of hiPSCs, variegation effects and residual transgene expression of the viral vectors used to induce

reprogramming (Soldner et al., 2009) and genetic alterations introduced during the reprogramming process (Gore et al., 2011; Hussein et al., 2011). Variable genetic background presents a particularly significant impediment to in vitro disease modeling approaches because it is not possible to control for effects from genetic modifier loci. Even mutations that cause the most prevalent monogenic diseases, including sickle cell anemia, cystic fibrosis, and dominant forms of familial Parkinson's disease (PD), are susceptible to significant epistatic effects of genetic background that result in incomplete penetrance and variable age of onset and disease progression (Lees et al., 2009; Summers, 1996).

Therefore, for the disease in a dish approach to be successful, it is essential to set up experimental systems in which the disease-causing genetic lesion of interest is the sole modified variable. However, the unresolved problem of genetically manipulating pluripotent human cells has prevented the creation of such genetically defined human model systems. Recently, we and others used engineered zinc finger nucleases (ZFNs) to drive efficient targeted integration of selectable markers into hESCs and hiPSCs (Hockemeyer et al., 2009; Zou et al., 2009). Employing this technology (referred to as "genome editing"), we present here a generally applicable solution to this key problem by demonstrating the generation of a panel of isogenic disease and control cell lines from hESCs and hiPSCs that differ exclusively at well-validated susceptibility variants for PD by genetically modifying single base pairs in the α-synuclein gene.

PD, the second most common late age onset neurodegenerative disorder, is characterized primarily by major loss of nigrostriatal dopaminergic neurons and the presence of proteinacious inclusion bodies (Lewy bodies) in affected cells. The discovery of mutations linked to rare forms of familial PD, such as dominant mutations in α-synuclein (A53T, E46K, A30P), the major component of Lewy bodies, has provided vital clues in understanding the molecular pathogenesis not only of the rare familial, but also of the more prevalent sporadic forms of the disease (Lees et al., 2009; Schulz, 2008). However, cellular and transgenic animal models expressing such mutants only partially recapitulate PD pathology (Dawson et al., 2010). In order to develop a genetically defined human in vitro model of PD, we sought to generate a panel of control and disease-related cell lines by either deriving hiPSCs from a patient carrying the A53T (G209) α-synuclein mutation followed by the correction of this mutation or, alternatively, by generating either the A53T (G209A) or E46K (G188A) mutation in the genome of wild-type hESCs.

RESULTS

Insertion of Disease-Causing A53T (G209A) α-Synuclein Mutation into hESCs

Genome editing with engineered ZFNs relies on a double-strand break (DSB) introduced by the nucleases. The ability to precisely target DSB to an investigator-specified site is critical because point mutations are transferred with maximal efficiency from episomal donors into the position of the DSB itself (Elliott et al., 1998; Goldberg et al., 2010). We engineered a panel of ZFNs that introduces a DSB precisely at nucleotide base 209 (site of A53T mutation) in exon 3 of the α-synuclein gene (Figures 1A and 1B and Table S1 and Table S2 available online). Screening of the ZFNs in transformed human cells demonstrated editing of up to 18% of α-synuclein alleles precisely at the intended site (Figure 1A).

Guided by our previous results on highly efficient targeted integration of genes in hESCs and hiPSCs (Hockemeyer et al., 2009), we initially considered a drug selection-based strategy to introduce the PD-causing A53T (G209A) mutation into the endogenous α-synuclein locus in hESCs. However, for many disease-related mutations that are located within protein-coding exons, including α-synuclein A53T (G209A), the same approach cannot be used because insertion of the selection marker would disrupt the expression of the targeted gene. We therefore devised an alternative strategy based on the insertion of a loxP site flanked puromycin resistance gene in the adjacent intron 23 bases downstream of the A53T α-synuclein mutation and the DSB (Figure 1B). For this gene editing strategy, a correct targeting event followed by Cre-recombinase-mediated excision of the selection cassette is expected to result in a single base pair change that creates the A53T (G209A) mutation in exon 3 of α-synuclein, with a remaining single loxP site in the following intron (Figure 1B).

The targeting donor construct (Syn-A53T-loxP-pGK-puro-loxP) comprising ~600 bp homology on each side of the ZFN-targeted site carrying the A53T (G209A) mutation (Figure 1B), together with four distinct ZFN pairs (Table 1, Figure 1A, Table S1, and Table S2), were electroporated into two different hESC lines (BGO1 and WIBR3). Southern blot analysis of individual single-cell-derived puromycin-resistant clones using probes 5′ and 3′ external to the donor homology region demonstrated the disruption of the genomic locus and integration of the targeting donor vector with a frequency of at least 25% (Figure 1C, Figure S1A, and Table 1). Further analysis using an internal probe against the 3′ targeting arm of the donor vector (Figure S1B) and against the ampicillin resistance gene (Figure S1C) revealed integrations of additional donor-derived vector sequences into the target locus, presumably via a hybrid homology directed repair (HDR)-end-joining-based process such as described previously (Richardson and Jasin, 2000).

Three out of 336 puromycin-resistant clones showed the correct modification of the targeted genomic locus by Southern blot (Figure 1C, Figure S1, and Table 1), which was further confirmed by sequencing after Cre-mediated excision of the selection cassette (Figure 1D). Two out of the three clones carried a small deletion in the second allele as a result of ZFN-mediated gene disruption. The correctly targeted clone with a nondisrupted wild-type allele (WIBR3-SNCA$^{A53T/WT}$-1A/-1C) displayed a normal karyotype (Figure S1D) and maintained a pluripotent state, as indicated by the uniform expression of pluripotency-specific marker proteins (Figure 1E) and the ability to form teratomas comprising cell types originating from all three developmental germ layers (Figure 1F). The stable integration of the transiently transfected ZFN or Cre-recombinase-expressing plasmids was excluded by Southern blot analysis (Figure S3). Furthermore, using an embryoid body (EB)-based protocol to induce neural differentiation, we were able to efficiently derive dopaminergic thyrosine hydroxylase (TH)-expressing neurons

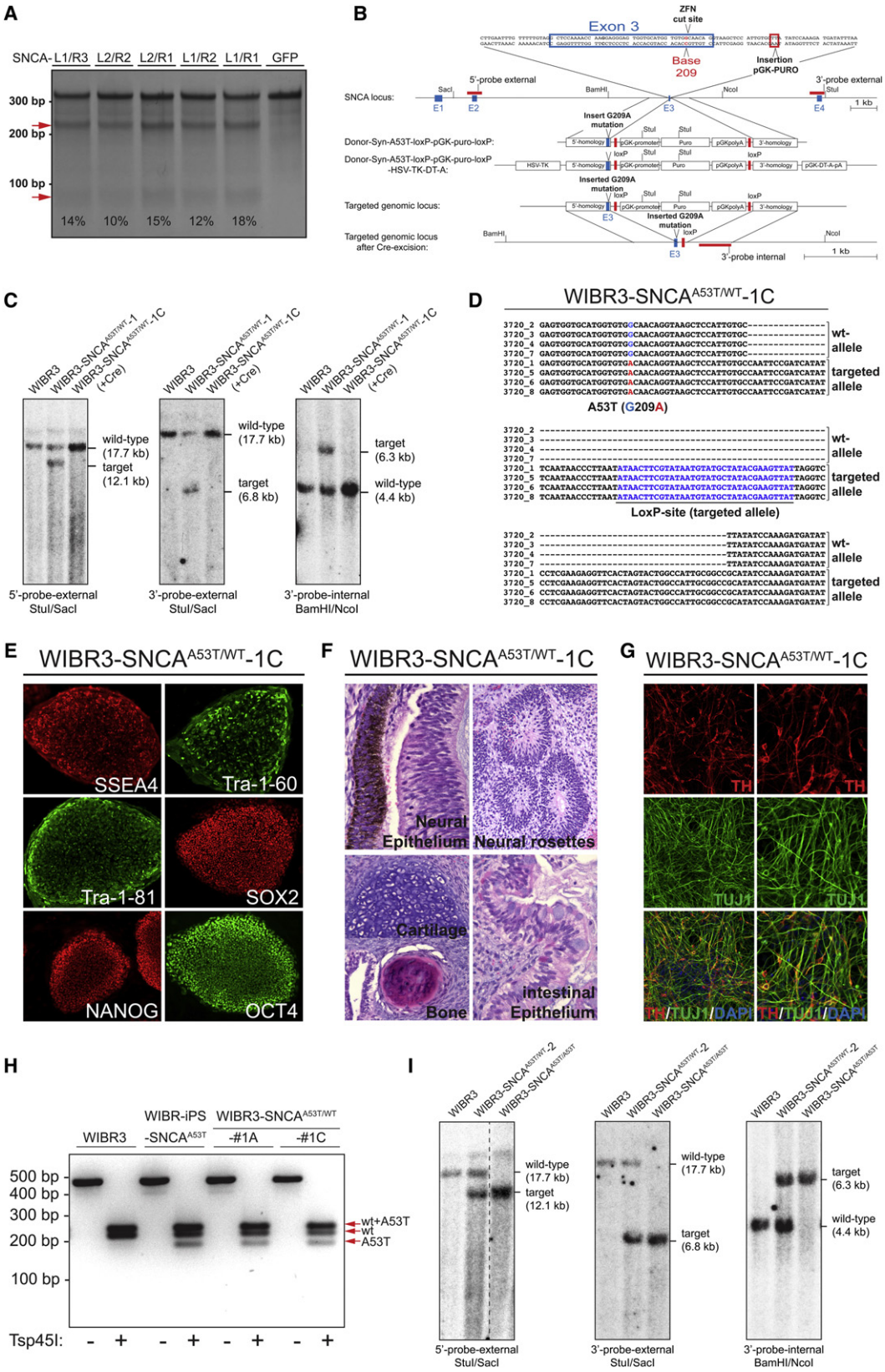
A
SNCA- L1/R3 L2/R2 L2/R1 L1/R2 L1/R1 GFP
300 bp
200 bp
100 bp
14% 10% 15% 12% 18%
B
ZFN cut site
Exon 3
Base 209
Insertion pGK-PURO
SNCA locus:
5'-probe external
3'-probe external
SacI
BamHI
NcoI
StuI
E1
E2
E3
E4
1 kb
Insert G209A mutation
Donor-Syn-A53T-loxP-pGK-puro-loxP:
Donor-Syn-A53T-loxP-pGK-puro-loxP -HSV-TK-DT-A:
Targeted genomic locus:
Inserted G209A mutation
Targeted genomic locus after Cre-excision:
3'-probe internal
C
WIBR3
WIBR3-SNCA A53T/WT-1
WIBR3-SNCA A53T/WT-1C (+Cre)
wild-type (17.7 kb)
target (12.1 kb)
target (6.8 kb)
target (6.3 kb)
wild-type (4.4 kb)
5'-probe-external StuI/SacI
3'-probe-external StuI/SacI
3'-probe-internal BamHI/NcoI
D
WIBR3-SNCA A53T/WT-1C
wt-allele
targeted allele
A53T (G209A)
LoxP-site (targeted allele)
E
WIBR3-SNCA A53T/WT-1C
SSEA4
Tra-1-60
Tra-1-81
SOX2
NANOG
OCT4
F
WIBR3-SNCA A53T/WT-1C
Neural Epithelium
Neural rosettes
Cartilage
Bone
intestinal Epithelium
G
WIBR3-SNCA A53T/WT-1C
TH
TUJ1
DAPI
H
WIBR-iPS
WIBR3
WIBR3-SNCA A53T
-SNCA A53T
-#1A
-#1C
500 bp
400 bp
300 bp
200 bp
100 bp
wt+A53T
wt
A53T
Tsp45I: - + - + - + - +
I
WIBR3
WIBR3-SNCA A53T/WT-2
WIBR3-SNCA A53T/A53T
wild-type (17.7 kb)
target (12.1 kb)
target (6.8 kb)
target (6.3 kb)
wild-type (4.4 kb)
5'-probe-external StuI/SacI
3'-probe-external StuI/SacI
3'-probe-internal BamHI/NcoI

from the targeted hESC line (Figure 1G). To verify that the loxP site remaining after Cre-mediated excision of the selection cassette does not interfere with the splicing or gene expression of α-synuclein, we differentiated the parental and targeted hESC lines into neurons in order to induce expression of α-synuclein. Mutation analysis RT-PCR (Polymeropoulos et al., 1997) confirmed that the levels and ratio of expression of the wild-type and the A53T-mutated transcript in the targeted cell line were similar to those observed in neurons derived from A53T patient-specific hiPSCs (WIBR-iPS-SNCA$^{A53T(1lox)}$) (Figure 1H).

In order to increase the targeting efficiency by reducing non-targeted integrations of the donor vector, as well as integration of donor vector sequences that are outside of the homology arms at the site of ZFN cleavage, we employed a positive-negative selection strategy (Capecchi, 1989) by incorporating the herpes simplex virus thymidine kinase (HSV-TK) and diphtheria toxin A-chain (DT-A) into the vector backbone (Figure 1B). Using this strategy, 9 out of 41 puromycin- and ganciclovir-resistant colonies resulted in a correctly targeted allele (Figure 1I and Table 1). Four of these clones had no disruption of the second wild-type allele, and 1 out of the 41 clones resulted in correct targeting and insertion of the A53T (G209A) mutation into both alleles (WIBR3-SNCA$^{A53T/A53T}$). The targeted clones initially identified by Southern blot analysis were confirmed by sequencing of the genomic locus (data not shown). None of the clones integrated the transiently transfected ZFNs (Figure S3). This single step biallelic modification of a disease-relevant locus represents a unique tool to study the role of mutant α-synuclein in the absence of the wild-type protein. Individuals that are homozygous for this mutation have not been described, and the study of homozygous mutant cells may provide new insights into the pathogenesis of PD.

Insertion of the A53T (G209A) Point Mutation into the α-Synuclein Gene without Drug Selection

The experiments described thus far, though successful in transferring a desired point mutation to the native locus, required the integration of a selectable marker into a neighboring intron. Dependent on the location of the desired editing events relative to intron/exon junction, such strategy may not be applicable to all genes; in addition, whereas the selectable marker can be excised using Cre-recombinase, the remaining loxP site represents an additional nonrequired genetic alteration with possible unpredictable effects. We therefore turned to an approach aimed at generating genetically pristine hESCs that contain no exogenous sequences other than the edited base (Urnov et al., 2005) for introducing the disease-causing point mutation (Figure 2A). Given the high gene editing activity of the ZFNs (Figure 1A, Figure S1A, and Table 1), we constructed a donor vector lacking a selection cassette, consisting only of ~1 kb homology flanking the ZFN cleavage site carrying the A53T (G209A) point mutation in order to insert the mutation in the endogenous α-synuclein locus in hESCs (Figure 2A). The hESC line BGO1 was electroporated with the donor construct together with ZFNs and an eGFP-expressing plasmid, which allows transfected cells to be enriched by fluorescence-activated cell sorting (FACS). Single-cell-derived colonies derived from this enriched pool were screened by Southern blot analysis using an A53T (G209A) allele-specific Tsp45I restriction digest. Three out of 240 BGO1 clones showed the A53T (G209A) allele-specific restriction pattern, indicative of an accurate genetic alteration event resulting in a A53T (G209A) mutation at the endogenous genomic locus (Figure 2B). Further analysis by PCR genotyping (Figure 2C) and sequencing of the genomic locus (Figure 2D) confirmed one correctly targeted clone (Table 1) with the expected single base pair change of nucleotide 209 on one allele and an unaffected

Figure 1. ZFN-Mediated Insertion of the A53T (G209A) α-Synuclein Mutation in hESCs Using a Drug Selection-Based Targeting Strategy

(A) Screening of ZFNs directed against nucleotide 209 of exon 3 of human α-synuclein. ZFN-mediated disruption of target locus was measured by the Surveyor/Cel-1 assay. Red arrows indicate expected Cel-1 digest products. The frequency of gene disruption of each ZFN pair is indicated below each lane (GFP indicates GFP-transfected negative control). All ZFNs were linked to wild-type FokI except pair SNCA-L1/R3, which was linked to an obligate heterodimer form of the Fok1 endonuclease (ELD-KKR).

(B) Schematic overview depicting the genomic α-synuclein locus (*SNCA*) and the targeting strategy showing exons (blue boxes), restriction sites, and location of external and internal Southern blot probes (red bars). Enlarged sequence indicates ZFN-induced cut site at base 209 in exon 3 of α-synuclein (red base pair) and insertion site of loxP-site-flanked pGK-puro selection cassette (red box). Shown below is a schematic of the donor plasmid design for either positive selection (Syn-A53T-loxP-pGK-puro-loxP) or positive-negative selection (Syn-A53T-loxP-pGK-puro-loxP-HSV-TK-DT-A) and targeted genomic locus before and after Cre-excision of the selection cassette. Donor plasmids comprise ~600 bp homology on each side of the ZFN cut. pGK-promoter, phosphoglycerol kinase promoter; puro, puromycin resistance gene; pGKpolyA, polyadenylation sequence; HSV-TK, herpes simplex virus thymide kinase; pGK-DT-A-pA, diphtheria toxin A-chain.

(C) Southern blot analysis of hESC line WIBR3 targeted with donor plasmid Syn-A53T-loxP-pGK-puro-loxP before (WIBR3-SNCA$^{A53T/WT}$-1) and after (WIBR3-SNCA$^{A53T/WT}$-1C) Cre-mediated excision of the selection cassette. Genomic DNA was digested with indicated enzymes and hybridized with the external 3′ and 5′ probe and internal 3′probe. Fragment sizes for each digest are indicated.

(D) Sequencing of genomic α-synuclein locus in hESC line WIBR3-SNCA$^{A53T/WT}$-1C showing either wild-type (G209, blue base) or targeted mutant (A209, red base) sequence. Targeted allele contains the remaining loxP site after Cre-mediated excision of selection cassette.

(E) Immunofluorescence staining of WIBR3-SNCA$^{A53T/WT}$-1C for the pluripotency markers OCT4, NANOG, SOX2, Tra-1-60, Tra-1-81, and SSEA4.

(F) Hematoxylin and eosin staining of teratoma sections generated from WIBR3-SNCA$^{A53T/WT}$-1C cells.

(G) Immunofluorescence staining of neuronal cultures derived from WIBR3-SNCA$^{A53T/WT}$-1C cells 10 days after induction of differentiation for neuron-specific class III β-tubulin (TUJ1; green) and the dopaminergic neuron-specific marker tyrosine hydroxylase (TH; red).

(H) Mutation analysis RT-PCR of α-synuclein transcript (± Tsp45I restriction digest) in indicated cell lines. (A53T mutation creates additional Tsp45I restriction site.) Expected fragment size after Tsp45I digest: wild-type transcript, 249/218/24/9 bp; A53T transcript, 249/185/33/ 24/9 bp (A53T- and wild-type [WT]-derived restriction fragments are indicated by red arrows).

(I) Southern blot analysis of WIBR3 cells targeted with donor plasmid Syn-A53T-loxP-pGK-puro-loxP-HSV-TK-DT-A after positive-negative selection. Genomic DNA was digested with indicated enzymes and hybridized with the external 5′ and 3′ probe and internal 3′probe. Fragment sizes for each digest are indicated (WIBR3-SNCA$^{A53T/WT}$-2 line shows correct targeting of one allele; WIBR3-SNCA$^{A53T/A53T}$ line shows correct targeting of both alleles).

Table 1. Summary of ZFN-Mediated Genome Editing Experiments and Analyzed Clones

Cell Line	Donor Vector/ ssODN	ZFN Pair	Number of Clones Analyzed	Number of Clones with Modified Target Locus	Number of Clones with Correctly Targeted Allele (Second Allele Disrupted)	Number of Correctly Targeted/ Analyzed Clones	Number of Off-Target Modifications/ Tested Sites	Cell Line Designation
BGO1	Donor-Syn-A53T-loxP-pGK-puro-loxP	ZFN L1/R1 ZFN L2/R1 ZFN L1/R2 ZFN L2/R2	60 60 60 60	17[a] 18[a] 17[a] 23[a]	1 (1) 1 (1) 	0/240		
WIBR3	Donor-Syn-A53T- loxP-pGK-puro-loxP	ZFN L1/R1	96	12[a]	1 (0)	1/96	0/38	WIBR3-SNCA$^{A53T/WT}$ 1A,1B,1C[d]
WIBR3	Donor-Syn-A53T- loxP-pGK-puro-loxP-HSV-TK-DT-A (positive-negative selection)	ZFN L1/R3	41	one allele: 17[a] both alleles: 2[a]	9 (5) 2 (1)	4/41 1/41	0/24[f] 0/12	WIBR3-SNCA$^{A53T/WT}$ 2,3,4,5 WIBR3-SNCA$^{A53T/A53T}$
WIBR3	ssODN-E46K	ZFN L1/R3	480	4[g]	4 (0)	4/480	nd	WIBR3-SNCA^{E46K} 1,2,3,4
BGO1	Donor-Syn-A53T (no selection)	ZFN L1/R1	240	3[b]	2 (1)	1/240	0/38	BGO1-SNCA$^{A53T/WT}$
BGO1	ssODN-E46K	ZFN L1/R3	240	1[g]	1 (0)	1/240	nd	BGO1-SNCA^{E46K}
WIBR-iPS-SNCA^{A53T}-5	Donor-Syn-WT (no selection)	ZFN L1/R1	240	6[c]	2 (1)	1/240	0/38	WIBR-iPS-SNCA$^{A53T-Corr}$ 1,2,3,4,5[e]

[a] Homologous and nonhomologous integration of donor vector (as analyzed in Figure S1).
[b] Insertion of A53T (G209A) mutation, as analyzed by Southern blot after TSP45I digest, genomic PCR mutation analysis, and sequencing.
[c] Loss-of-A53T (G209A) mutation, as analyzed by Southern blot after TSP45I digest, genomic PCR mutation analysis, and sequencing.
[d] 1A, 1B, and 1C represent different subclones of WIBR3-SNCA$^{A53T/WT}$-1 after Cre-mediated excision of selection cassette.
[e] 1, 2, 3, 4, and 5 represent different subclones of WIBR-IPS-SNCA$^{A53T-Corr}$ after Cre-mediated excision of the reprogramming transgenes.
[f] 0/12 off-target modifications in lines WIBR3-SNCA$^{A53T/WT}$-2 and WIBR3-SNCA$^{A53T/WT}$-3.
[g] PCR mutation analysis-based screening strategy for E46K (G188A) mutation is not sensitive for modifications at the site of ZFN-induced DSB (base 209).

second allele resulting in a A53T mutated cell line on a genetic BGO1 background (BGO1-SNCA$^{A53T/WT}$). The targeted cell line maintained a pluripotent state, as indicated by the uniform expression of pluripotency-specific markers (Figure 2E) and the ability to form teratomas (Figure 2F) and differentiate into dopaminergic neurons in vitro (Figure 2G). The stable integration of the ZFNs and GFP expression plasmids was excluded by Southern blot analysis (Figure S3).

Insertion of the PD-Causing E46K (G188A) Point Mutation into α-Synuclein in hESCs Using Single-Stranded Oligodeoxynucleotides

Recent studies suggest that short single-stranded oligodeoxynucleotides (ssODNs) instead of double-stranded donor plasmids can be used as an alternative DSB repair template for ZFN-driven genome editing (Chen et al., 2011; Radecke et al., 2006, 2010). As it has been shown that point mutations can be transferred distant from the ZFN-induced DSB (Elliott et al., 1998; Goldberg et al., 2010), we wanted to test the possibility of introducing a second PD-causing mutation (E46K/G188A) into exon 3 of α-synuclein (Zarranz et al., 2004) and therefore designed a 114 bp ssODN carrying the disease-relevant G188A base pair change, located 21 bases upstream of the A53T (G209A) mutation (Figure 3A). The hESC lines BGO1 and WIBR3 were electroporated with ZFNs and an eGFP-expressing plasmid together with the ssODNs instead of a double-stranded donor vector (Figure 3A). Individual single-cell-derived clones from FACS-sorted eGFP-expressing cells were screened by PCR followed by the mutation-specific StyI restriction digest. Four out of 480 WIBR3 clones and one out of 240 BGO1 clones showed the E46K (G188A) allele-specific loss of the StyI restriction site as verified by PCR genotyping (Zarranz et al., 2004) and Southern blot analysis (Figures 3B and 3C), indicative of the accurate genetic alteration of the endogenous α-synuclein genomic locus. Further analysis by sequencing of the genomic locus confirmed the correct insertion of the E46K (G188A) mutation without any additional alteration of the wild-type or mutated allele adjacent to the ZFN cleavage site (Figures 3D and 3E). The targeted cell lines maintained a pluripotent state, as indicated by the uniform expression of pluripotency-specific marker proteins (Figures 3F and 3G). The efficiency of correctly genome edited clones using ssODNs as template was comparable to that of using double-stranded donor plasmids (Table 1).

Genetic Repair of the A53T (G209A) α-Synuclein Mutation in PD Patient-Derived hiPSCs

Fibroblasts obtained from a patient carrying the A53T (G209A) α-synuclein mutation were reprogrammed using previously described doxycycline-inducible and Cre-recombinase-excisable lentiviral vectors (Hockemeyer et al., 2008; Soldner et al., 2009). The resulting hiPSCs before (WIBR-iPS-SNCA$^{A53T(2lox)}$) (Figure 4) and after Cre-mediated excision of the reprogramming factors (WIBR-iPS-SNCA$^{A53T(1lox)}$) (Figure S2) displayed all basic properties of pluripotent cells, as indicated by the uniform expression of the pluripotency marker proteins (Figure 4A and Figure S2B), the ability to form teratomas (Figure S2C), and a normal karyotype (Figure 4B). Sequencing of the genomic α-synuclein locus confirmed the A53T (G209A) mutation in the patient-derived hiPSCs (Figure 4D). Furthermore, the cells were shown to differentiate into TH-expressing dopaminergic neurons (Figure 4E).

In order to genetically repair the A53T (G209) mutation in the PD patient-derived hiPSCs, we employed a selection-free targeting strategy, as described above for hESCs, with the only difference of using a wild-type sequence-containing donor vector (Figure 2A). Six out of 240 WIBR-iPS-SNCA^{A53T} clones demonstrated the loss of the A53T-specific Tsp45I restriction site by Southern blot screening, which is either the result of a ZFN-induced DSB followed by nonhomologous error-prone end-joining or HDR-based correction of the allele (Figure 5A). Further analysis by PCR genotyping (Figure 5B) and sequencing of the genomic locus (Figure 5C) confirmed one correctly repaired patient-derived hiPSC line (WIBR-iPS-SNCA$^{A53T-Corr}$; Table 1) with the expected single base pair change of nucleotide 209 of α-synuclein. Finally, to prevent uncontrollable effects from residual expression of the reprogramming transgenes (Soldner et al., 2009), we excised the reprogramming vectors from the corrected patient-derived hiPSCs (Figure S2D), which subsequently displayed a normal karyotype (Figure 5E), maintained a pluripotent state as indicated by the uniform expression of the pluripotency markers (Figure 5F), and displayed the ability to form teratomas (Figure 5G). Stable integration of ZFNs, Cre-recombinase, and GFP expression plasmids was excluded by Southern blot analysis (Figure S3). The genetic repair of the A53T mutation in the patient-derived hiPSCs did not compromise the ability to differentiate into TH-expressing dopaminergic neurons (Figure 5H). To further validate accurate editing of the α-synuclein locus in the repaired patient-derived hiPSC line (WIBR-iPS-SNCA$^{A53T-Corr}$), we performed mutation analysis RT-PCR of α-synuclein after neuronal differentiation, confirming the loss of expression of the mutated A53T (G209A) transcript (Figure 5D).

Genome-wide Analysis of Engineered ESCs and iPSCs

A potential limitation of ZFN-mediated genome editing is the induction of DNA strand breaks at sequences other than the intended target site. To examine off-target modifications in the edited cell lines, we initially determined the DNA binding specificity for each ZFN employed in this study by SELEX analysis, as described previously (Hockemeyer et al., 2009; Perez et al., 2008) (Table S3). This allows for the identification of the most probable off-target cleavage sites genome-wide (Table S4). A Surveyor endonuclease (Cel-1) assay was subsequently performed to reveal any potential nonhomologous end-joining (NHEJ)-mediated indels for a large panel of putative off-target sites in several of our edited cell lines (Table 1 and Figure S4). Although this analysis has revealed rare bona fide off-target modification by ZFNs in other studies (Hockemeyer et al., 2009; Perez et al., 2008), we saw no evidence of off-target genome disruption at any of the examined loci (Table1 and Figure S4).

It is well established that prolonged culture of hESCs can lead to adaption such as increased growth rate, reduced apoptosis, and the acquisition of chromosomal abnormalities such as copy number variations (CNVs) (Laurent et al., 2011; Närvä et al., 2010). More recently, it has been proposed that the reprogramming process itself compromises genomic integrity and leads to the accumulating of CNVs and somatic mutations (Gore et al., 2011; Hussein et al., 2011). Although all of our tested cell lines showed a normal karyotype after genome editing as determined by conventional karyotyping, the low resolution of this technology excludes the detection of smaller CNVs, which are considered a major source for human genome variability and particularly important in the context of genome editing. Such genetic modifications involve the induction of DNA double-strand breaks and clonal events, which are thought to increase the chance for additional genomic alterations. We therefore performed high-resolution genome-wide CNV analysis using an Affymetrix SNP 6.0 array, as described previously (Hussein et al., 2011; Närvä et al., 2010), on three pairs of isogenic parental and genetically modified cell lines. We identified, on average, 77 CNVs with an average size of 158 kb per cell line (Table S5). For human ES cell lines, this is slightly higher than described previously and may be due to technical variability such as low sample or higher passage number of the cell lines used in this study (between passage P25 and P60 for hESCs and P22 and P40 for hiPSCs). Sixty-three percent of the identified CNVs (number and total genomic area) overlapped between isogenic pairs using pairwise comparison before and after ZFNs-mediated genome modification (Figures S5A–S5E). In contrast, we observed only 35% overlap of CNVs between genetically unrelated samples (Figures S5A–S5E). This degree of overlap is comparable to previously published hESC data comparing identical cell lines at different passage numbers (Figures S5D and S5E) (Närvä et al., 2010). Furthermore, comparing average number and total genome area of CNVs before and after ZFN-mediated gene targeting did not reveal any additional change other than that observed during regular hESCs in culture (Figure S5F). Consistent with previous reports (Närvä et al., 2010), our analysis confirms that hESCs and hiPSCs contain a higher number of CNVs than the normal human genome independent of the genome editing procedure—probably acquired during hESC derivation, the reprogramming process, and prolonged cell culture. Moreover, we conclude that the Cre-recombinase-mediated excision of the reprogramming factors and ZFN-mediated genome editing did not substantially increase the level of genomic alterations. To further validate that the genome editing approach did not induce major genetic or epigenetic alterations that would result in aberrant gene expression profiles, we performed whole-genome expression

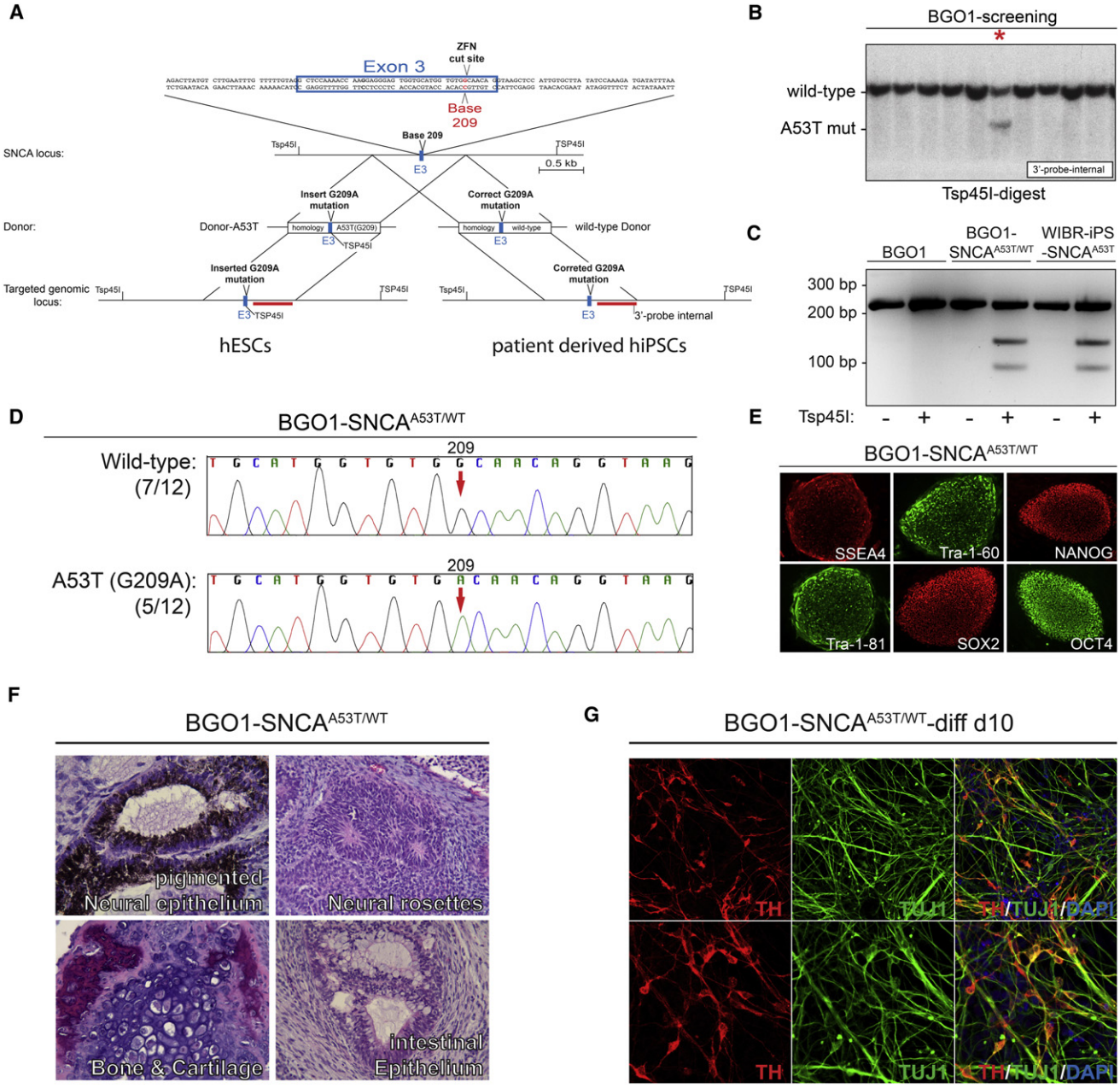

Figure 2. ZFN-Mediated Insertion of the A53T α-Synuclein Mutation in hESC Line BGO1 without Drug Selection

(A) Schematic overview depicting the genomic α-synuclein (*SNCA*) locus and the targeting strategy showing exons (blue boxes), restriction sites, and location of internal Southern blot probe (red bars). Enlarged sequence indicates ZFNs induced cut site at base 209 in exon 3 of α-synuclein (red base pair). Shown below is a schematic of donor plasmid design and targeted genomic locus for either insertion (Donor-A53T) or correction (wild-type Donor) of A53T (G209A) α-synuclein mutation. Donor plasmids contain ~1 kb homology to the targeting site.

(B) Southern blot screening (3′ internal probe) of BGO1 cells for targeted insertion of A53T (G209A) mutation (Donor-A53T). Genomic DNA was digested using an A53T (G209A)-allele-specific Tsp45I restriction digest (A53T mutation creates additional Tsp45I restriction site). Expected fragment sizes: wild-type allele, 2.96 kb; A53T allele, 1.55 kb. 3′ internal Southern blot probe excludes additional nonhomologous integration of the donor vector. Red asterisk indicates clone with additional Tsp45I restriction site indicative of insertion of A53T mutation.

(C) PCR mutation analysis of α-synuclein locus (± Tsp45I restriction digest) in patient-derived hiPSCs (WIBR-iPS-SNCA^{A53T}) and targeted hESCs (BGO1-SNCA$^{A53T/WT}$ represents clone marked by red asterisk in B). Fragment sizes (+ Tsp45I): wild-type allele, 219 bp; A53T allele, 131/88 bp.

(D) Sequencing of genomic α-synuclein locus in targeted hESC clone BGO1-SNCA$^{A53T/WT}$ displaying either wild-type allele (G209 in 7 out of 12 sequences) or targeted mutant A53T allele (A209 in 5 out of 12 sequences).

(E) Immunofluorescence staining of BGO1-SNCA$^{A53T/WT}$ for the pluripotency markers OCT4, NANOG, SOX2, Tra-1-60, Tra-1-81, and SSEA4.

(F) Hematoxylin and eosin staining of teratoma sections generated from BGO1-SNCA$^{A53T/WT}$ cells.

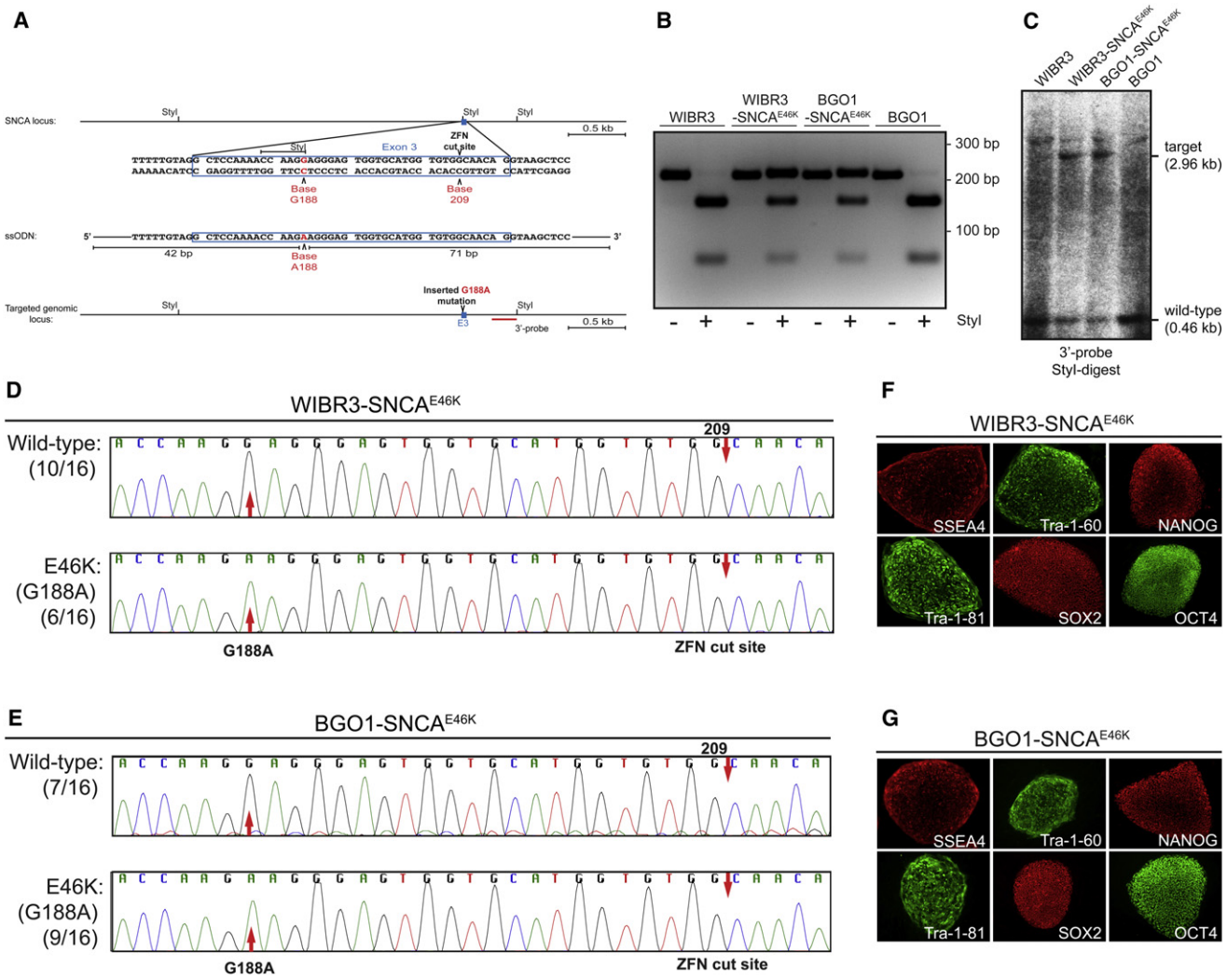

Figure 3. ZFN-Mediated Insertion of the E46K α-Synuclein Mutation in hESCs Using ssODNs

(A) Schematic overview depicting the genomic α-synuclein (*SNCA*) locus and the targeting strategy showing exon 3 (blue boxe), restriction sites, and location of Southern blot probe (red bar). Enlarged sequence indicates ZFNs induced cut site at base 209 in exon 3 of α-synuclein and the site of the E46K (G188A) mutation (red base pair). Shown below is a schematic of the 114 bp ssODN and the targeted genomic locus after insertion of E46K (G188A) α-synuclein mutation.

(B) PCR mutation analysis of α-synuclein locus (± StyI restriction digest) in hESC lines WIBR3 and BGO1 and targeted E46K hESC lines (WIBR3-SNCA^{E46K} and BGO1-SNCA^{E46K}). Fragment sizes (+ StyI): wild-type allele, 153/66 bp; E46K mutated allele, 219 bp.

(C) Southern blot analysis (3′ probe) of WIBR3 and BGO1 and targeted E46K hESC lines (WIBR3-SNCA^{E46K} and BGO1-SNCA^{E46K}) for targeted insertion of E46K (G188A) mutation. Genomic DNA was digested using an E46K (G188A) allele-specific StyI restriction digest (E46K mutation disrupts wild-type allele specific StyI restriction site). Expected fragment sizes: wild-type allele, 0.46 kb; E46K mutated allele, 2.96 kb.

(D) Sequencing of genomic α-synuclein locus in targeted hESC clone WIBR3-SNCA^{E46K} displaying either wild-type allele (G188 in 10 out of 16 sequences) or targeted mutant E46K allele (A188 in 6 out of 16 sequences).

(E) Sequencing of genomic α-synuclein locus in targeted hESC clone BGO1-SNCA^{E46K} displaying either wild-type allele (G188 in 7 out of 16 sequences) or targeted mutant E46K allele (A188 in 9 out of 16 sequences).

(F) Immunofluorescence staining of WIBR3-SNCA^{E46K} for the pluripotency markers OCT4, NANOG, SOX2, Tra-1-60, Tra-1-81, and SSEA4.

(G) Immunofluorescence staining of BGO1-SNCA^{E46K} for the pluripotency markers OCT4, NANOG, SOX2, Tra-1-60, Tra-1-81, and SSEA4.

analysis of undifferentiated pairs of parental and genetically modified cell lines. Despite very similar gene expression of all pluripotent cell lines, hierarchical cluster analysis showed that the influence of genetic background on gene expression is more significant than the genome editing because gene expression patterns of pairs of parental and genome-edited cell lines are more closely correlated than genetically independent cell lines (Figure S5G).

(G) Immunofluorescence staining of neuronal cultures derived from BGO1-SNCA$^{A53T/WT}$ cells 10 days after induction of differentiation for neuron-specific class III β-tubulin (TUJ1; green) and the dopaminergic neuron-specific marker tyrosine hydroxylase (TH; red).

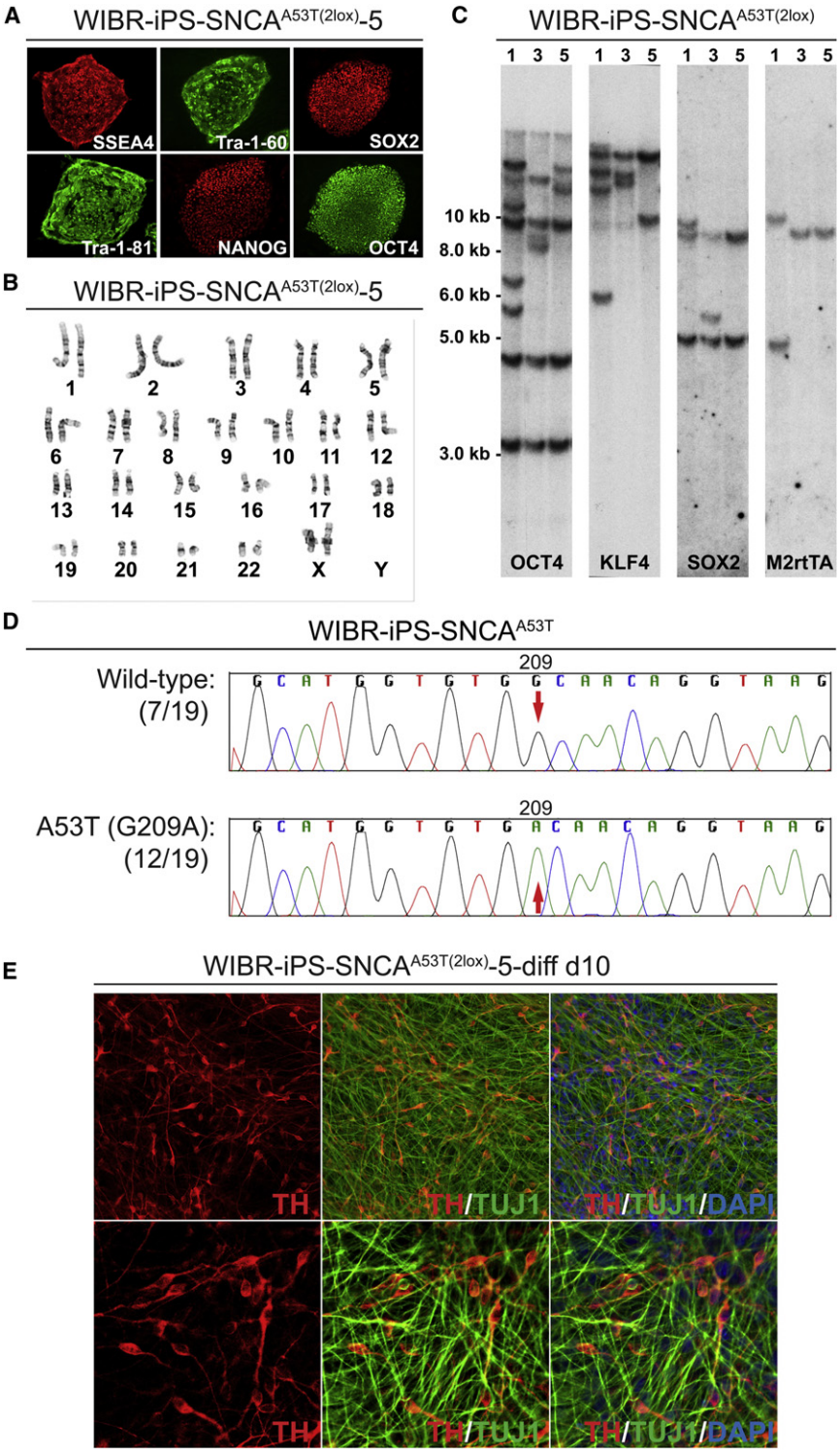

Figure 4. Derivation of Disease-Specific hiPSCs from PD Patient with A53T (G209A) α-Synuclein Mutation

(A) Immunofluorescence staining of PD patient-derived hiPSC line WIBR-iPS-SNCA$^{A53T(2lox)}$-5 for the pluripotency markers OCT4, NANOG, SOX2, Tra-1-60, Tra-1-81, and SSEA4.

(B) Cytogenetic analysis of patient-derived hiPSC line WIBR-iPS-SNCA$^{A53T(2lox)}$-5 showing a normal karyotype.

(C) Southern blot analysis of WIBR-iPS-SNCA$^{A53T(2lox)}$ clones. Genomic DNA was digested with XbaI and probed for proviral integrations with ^{32}P-labeled DNA probes against hOCT4, hKLF4, hSOX2, and M2rtTA. Southern blot analysis confirms independent clones based on individual proviral integration patterns.

(D) Sequencing of genomic α-synuclein locus in PD patient-derived hiPSC line WIBR-iPS-SNCA$^{A53T(2lox)}$-5 showing both wild-type allele (G209 in 7 out of 19 sequences) and mutant A53T allele (A209 in 12 out of 19 sequences).

(E) Immunofluorescence staining of neuronal cultures derived from hiPSC line WIBR-iPS-SNCA$^{A53T(2lox)}$-5 10 days after induction of differentiation for neuron-specific class III β-tubulin (TUJ1; green) and the dopaminergic neuron-specific marker tyrosine hydroxylase (TH; red).

DISCUSSION

Although transgenic animal models of disease and studying human cultured cells in a Petri dish are core technologies driving basic biomedical research, there are many instances in which these approaches only partially recapitulate the molecular and cellular changes observed in the patient. The ability to generate an unlimited supply of patient-derived, disease-relevant cell types using hiPSC technology has the potential to transform biomedical research of human disease. However, numerous challenges on the path to well-defined experimental in vitro systems must be resolved before realizing the full promise of this technology. One of the crucial limitations has been the inability to perform experiments under genetically defined conditions. Here, we present an elegant solution to this problem by combining the advantages of ZFN-mediated gene editing such as the ability to engineer ZFNs to target any locus in the genome (Urnov et al., 2010) and easy donor design, requiring only very short targeting homologies, with hESC and hiPSC technology. The recent demonstration of efficient gene editing in human pluripotent cell lines using transcription activator-like effector (TALE) nucleases as an alternative strategy to induce site-specific genomic DSBs will further expand the versatility of this approach (Hockemeyer et al., 2011).

Table 2 compares the strengths and the weaknesses of the four strategies described in this study. Although a gene-targeting vector using positive-negative selection represents the most efficient genome editing strategy, this approach requires the deletion of the selection cassette and therefore necessitates a second single-cell cloning step, adding time to generate the final targeted cell line. Another unavoidable consequence of the selection-based strategy is that it leaves a genetic footprint, such as a loxP site, close to the targeted genetic alteration. In contrast, the selection-free strategy, though less efficient, leaves no genetic footprint and involves only one cell cloning step and thus shortens the time required to generate the targeted cell line. The simplicity of synthesizing ssODN-based donors combined with the ability to transfer genomic alterations adjacent to the ZFN induced DSB greatly increases the versatility and applicability of the no-selection-based approach and may represent the most advantageous option for genome editing.

Here, we generated a panel of isogenic control and disease cell lines on several defined genetic backgrounds by either engineering the PD-related A53T or E46K mutation into hESCs or, inversely, repairing the mutation in PD-patient-derived hiPSCs by exclusively changing a single base pair without the need to alter the genome in any other way. Considering the broad influence of genetic background and the profound biological differences between individual hESCs and hiPSCs, such as the propensity to differentiate toward specific cell lineages (Bock et al., 2011; Boulting et al., 2011), this experimental system may overcome some of the shortcomings of conventional hiPSC approaches in identifying disease-related phenotypes. Robust disease-relevant in vitro phenotypes are fundamentally important to identify new drug targets or allow large-scale screening of genetic and small-molecule disease modifiers. The availability of genetically defined pairs of disease and control cell lines becomes even more significant in the context of unbiased genome-wide analysis in order to distinguish between genetic background noise and disease relevant effects, considering that the expression of ~5% of genes is thought to be linked to genetic variation (Montgomery et al., 2010; Pickrell et al., 2010).

Though biomedical research is likely to benefit substantially from in vitro disease modeling, the ultimate promise of iPSC technology, albeit at a very early stage of development, is the concept of cell replacement therapy in degenerative diseases using autologous cells (Daley and Scadden, 2008). Proof-of-principle experiments in the mouse (Hanna et al., 2007) have established the feasibility of treating monogenic diseases using the combined approach of derivation of disease-specific iPSCs followed by in vitro repair of the underlying genetic alteration and subsequent transplantation of corrected iPSC-derived cells. Similar approaches with human cells are currently hindered by the problem of efficient gene targeting required for repair of disease-causing genomic alterations (Daley and Scadden, 2008). The methods described here for genetically correcting a disease-causing point mutation in patient-derived hiPSCs should be widely applicable and important both for elucidating disease mechanism and for moving toward hiPSC-based cell replacement therapies.

EXPERIMENTAL PROCEDURES

HESC and hiPSC Derivation and Culture

HESC lines BG01 (NIH code: BG01; BresaGen, Inc., Athens, GA) and WIBR3 (Whitehead Institute Center for Human Stem Cell Research, Cambridge, MA) (Lengner et al., 2010) and hiPSCs were derived and maintained as described previously (Soldner et al., 2009) and in detail in the Extended Experimental Procedures. The patient biopsied harbors the A53T α-synuclein mutation and has been described previously (Golbe et al., 1996). All protocols were approved by the relevant Institutional Review Boards (Boston University Medical Campus; Massachusetts Institute of Technology) and Embryonic Stem Cell Research Oversight Committees (Whitehead Institute), and written informed consent was obtained before biopsy. All pluripotent cell lines have been characterized by conventional methods, which are described in detail in the Extended Experimental Procedures.

ZFN Design and ZFN Expression Plasmids

ZFNs against the human α-synuclein locus were designed using an archive of prevalidated two-finger modules, as described (Doyon et al., 2008; Miller et al., 2007; Perez et al., 2008; Urnov et al., 2005). Complete sequences of target sites of the zinc finger proteins are provided in Table S1 and Table S2. All ZFNs were linked to wild-type FokI, except pair SNCA-L1/R3, which was linked to an obligate heterodimer form of the Fok1 endonuclease (ELD-KKR) (Doyon et al., 2011; Miller et al., 2007; Perez et al., 2008). The ZFNs were tested by transient transfection into K562 cells to test for disruption of the wild-type α-synuclein allele. Disruption efficiency at the target locus was determined by Surveyor (Cel-1) endonuclease-based measurement of nonhomologous end-joining, as described (Miller et al., 2007; Perez et al., 2008) (primers used in Cel-1 analysis: SNCA-Cel1-FW, 5′-AAACTAGCTAATCAGCAATTTAAGGC-3; SNCA-Cel1-RW, 5′-AGCCCTCATTATTCTTGGCA-3). Analysis of off-target cleavage by ZFNs, which results in NHEJ-mediated indels, was performed essentially as described before (Doyon et al., 2008; Hockemeyer et al., 2009; Perez et al., 2008) and is described in detail in the Extended Experimental Procedures.

ZFN-Mediated Genome Editing of hESCs and hiPSCs

HESCs and hiPSCs were cultured in Rho-associated protein kinase (ROCK) inhibitor (Calbiochem; Y-27632) 24 hr prior to electroporation. Cells were harvested using 0.05% trypsin/EDTA solution (Invitrogen) and were resuspended in phosphate buffered saline (PBS). For drug selection-based gene editing, 1×10^7 cells were electroporated with 35 μg of donor plasmids (designed and assembled by F.S.) and 7.5 μg of each ZFN-encoding plasmid (Gene Pulser Xcell System, Bio-Rad: 250 V, 500 μF, 0.4 cm cuvettes). Cells were subsequently plated on DR4 MEF feeder layers in hESC medium supplemented with ROCK inhibitor for the first 24 hr. Ganciclovir (1×10^{-6} M) and/or puromycin selection (0.5 μg/ml) was started 72 hr after electroporation. For drug selection-free gene editing, 1×10^7 cells were electroporated with 30 μg of donor plasmids (designed and assembled by F.S.), 7.5 μg of each ZFN-encoding plasmid, and 10 μg of pEGFP-N1 (Clontech). For gene editing using ssODNs, 1×10^7 cells were electroporated with 7.5 μg of each ZFN-encoding plasmid and 15 μg of pEGFP-N1 (Clontech) together with 30 μg of ssODNs (5′-GACTTATGTCTTGAATTTGTTTTTGTAGGCTCCAAAACCAAGAAGGGAGTGGTGCATGGTGTGGCAACAGGTAAGCTCCATTGTGCTTATATCCAAAGATGATATTTAAAGTAT-3′; Integrated DNA Technologies, Iowa). Cells were maintained on MEF feeder layers for 72 hr in the presence of ROCK Inhibitor followed by FACS sorting (FACS-Aria; BD-Biosciences) of a single-cell suspension for eGFP-expressing cells and were subsequently plated at a low density in hESC medium supplemented with ROCK inhibitor for the first 24 hr. Individual colonies were picked and expanded 10–14 days after electroporation.

ACCESSION NUMBERS

Expression Microarray data and SNP 6.0 CNV array data have been submitted to the Gene Expression Omnibus (GEO) and are available under accession number GSE29774.

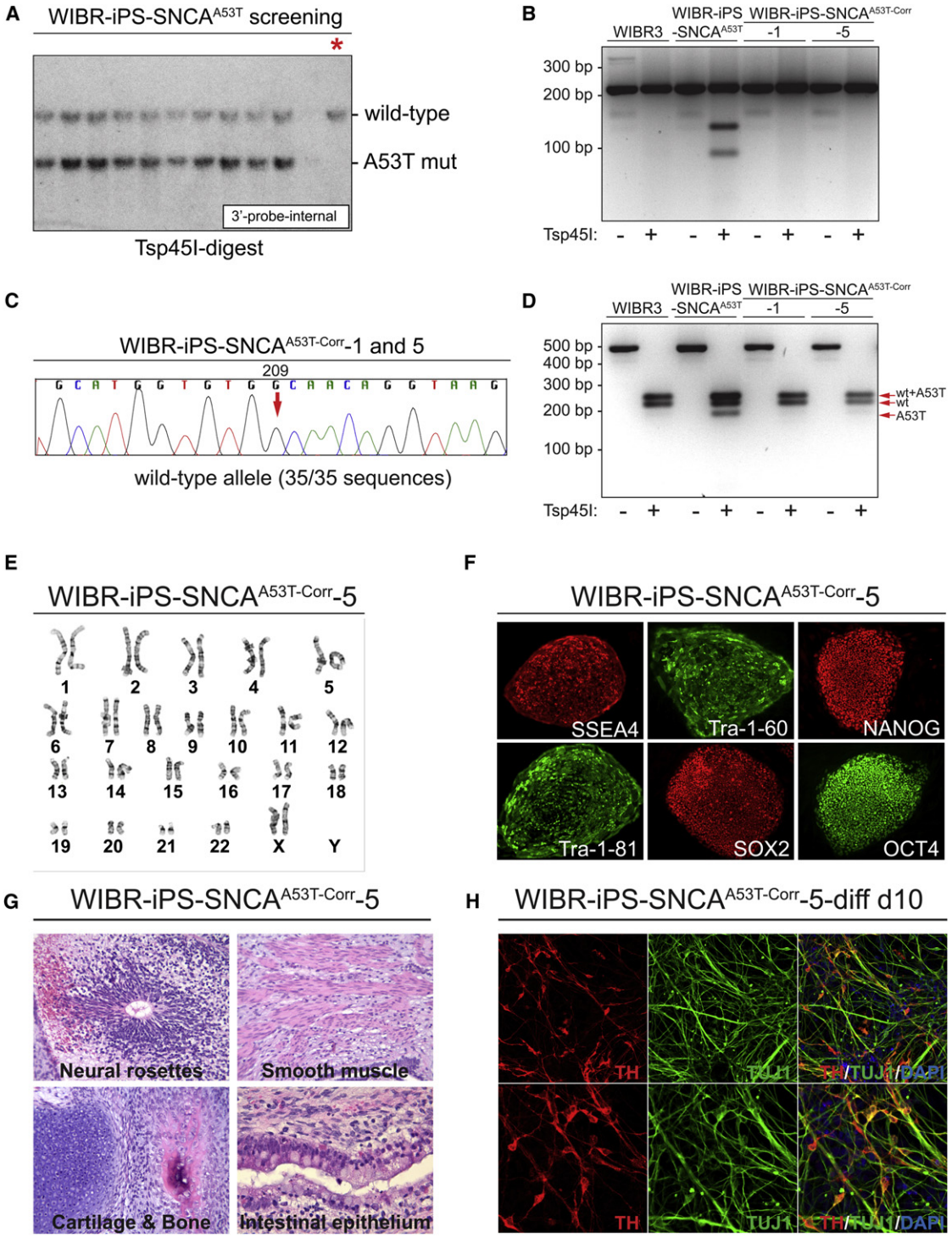

Figure 5. ZFN-Mediated Correction of A53T (G209A) Mutation in PD Patient-Derived hiPSCs

(A) Southern blot screening (3′ internal probe) of patient-derived hiPSCs (WIBR-iPS-SNCA^{A53T}) for correction of A53T (G209A) mutation (wild-type Donor). Genomic DNA was digested using an A53T (G209A) allele-specific Tsp45I restriction digest (A53T mutation creates additional Tsp45I restriction site). 3′ internal Southern blot probe excludes additional nonhomologous integration of the donor vector. Fragment sizes: wild-type allele, 2.96 kb; A53T allele, 1.55 kb. Red asterisk indicates clone with loss of Tsp45I restriction site, indicative of loss of A53T mutation.

(B) PCR mutation analysis of genomic α-synuclein locus (± Tsp45I restriction digest) in hESCs (WIBR3) and patient-derived hiPSCs before (WIBR-iPS-SNCA^{A53T}) and after correction (WIBR-iPS-SNCA$^{A53T-Corr}$-1 and -5, representing two subclones from clone marked by red asterisk in A). Fragment sizes (+Tsp45I): wild-type allele, 219 bp; A53T mutant allele, 131/88 bp.

Table 2. Comparison of the Four Different Targeting Strategies

Strategy	Donor	Targeting Steps	Time Required[a]	Efficiency[b]	Strengths	Drawbacks
Selection based	positive selection	2	8–16 weeks	+	high efficiency; use of multiple selection markers allows for targeting of both alleles	complex vector design; two clonal steps; genetic alteration (remaining loxP site)
	positive-negative selection	2	8–16 weeks	++	same as above	same as above
No selection	vector-based donor	1	4–8 weeks	+	one clonal step; no additional genetic alterations	complex vector design
	ssODN	1	4–8 weeks	+	in addition, easy donor design	

[a] Time between electroporation and identification of modified cell line.
[b] + ~ 1%; ++ ~ 10% (efficiencies may vary for different genes).

SUPPLEMENTAL INFORMATION

Supplemental Information includes Extended Experimental Procedures, five figures, and five tables and can be found with this article online at doi:10.1016/j.cell.2011.06.019.

ACKNOWLEDGMENTS

We thank Ping Xu and Tenzin Lungjangwa for technical support and Jessica Dausman, Kibibi Ganz, Ruth Flannery, and Dongdong Fu for their help with animal husbandry and processing of teratomas. We would like to thank Tom Volkert and Jeong-Ah Kwon of the Whitehead Genome Technology Core for their help with the CNV analysis; Nicki Watson of the W.M. Keck Microscopy Facility for help with confocal microscopy; and Patti Wisniewski and Chad Araneo of the Whitehead Institute FACS facility for their help with cell sorting. We thank Gladys Dulay for construction of ZFN vectors and Elo Leung for computational analysis for the off-target study. We thank all of the members of the Jaenisch lab for helpful discussions and comments on the manuscript. R.J. was supported by NIH grants R01-CA084198 and R37-HD045022. This research was supported, in part, by a Collaborative Innovation Award from the Howard Hughes Medical Institute. R.J. is an adviser to Stemgent and a cofounder of Fate Therapeutics. D.H. is a Merck Fellow of the Life Sciences Research Foundation. J.L., L.K.F., L.Z., F.D.U., P.D.G., H.S.Z., D.J., B.J.V., X.M., and E.J.R. are full-time employees of Sangamo BioSciences, Inc.

F.S. and R.J. designed the experiments and wrote the paper. A.W.C. performed computational analysis for gene expression and CNVs. D.H. provided assistance with hiPSC derivation. Q.G. analyzed all teratomas. R.A. provided assistance with molecular characterization of genome-edited pluripotent cells. V.K., L.I.G., R.H.M., and S.L. identified PD patient and provided patient-derived skin biopsy. L.Z. and D.G. designed the ZFNs; J.L. and L.K.F. tested the ZFNs; J.L., B.J.V., and X.M. performed the off-target analysis; J.L., X.M., F.D.U., and H.S.Z. analyzed data; J.L., E.J.R., P.D.G., and H.S.Z. designed and supervised ZFN assembly and characterization; J.L., F.D.U., P.D.G., and H.S.Z. contributed to manuscript preparation; F.S. performed all other experiments.

Received: January 31, 2011
Revised: May 9, 2011
Accepted: June 10, 2011
Published online: July 14, 2011

REFERENCES

Bock, C., Kiskinis, E., Verstappen, G., Gu, H., Boulting, G., Smith, Z.D., Ziller, M., Croft, G.F., Amoroso, M.W., Oakley, D.H., et al. (2011). Reference Maps of human ES and iPS cell variation enable high-throughput characterization of pluripotent cell lines. Cell *144*, 439–452.

Boulting, G.L., Kiskinis, E., Croft, G.F., Amoroso, M.W., Oakley, D.H., Wainger, B.J., Williams, D.J., Kahler, D.J., Yamaki, M., Davidow, L., et al. (2011). A functionally characterized test set of human induced pluripotent stem cells. Nat. Biotechnol. *29*, 279–286.

Brennand, K.J., Simone, A., Jou, J., Gelboin-Burkhart, C., Tran, N., Sangar, S., Li, Y., Mu, Y., Chen, G., Yu, D., et al. (2011). Modelling schizophrenia using human induced pluripotent stem cells. Nature *473*, 221–225.

Capecchi, M.R. (1989). Altering the genome by homologous recombination. Science *244*, 1288–1292.

Chen, F., Pruett-Miller, S., Huang, Y., Gjoka, M., Duda, K., Taunton, J., Collingwood, T.N., Frodin, M., and Davis, G.D. (2011). Genome editing using ssDNA oligonucleotides with zinc finger nucleases. Nat. Methods. 10.1038/nmeth.1653.

Daley, G.Q., and Scadden, D.T. (2008). Prospects for stem cell-based therapy. Cell *132*, 544–548.

(C) Sequencing of genomic α-synuclein locus in PD patient-derived hiPSCs after ZFN-mediated correction. Corrected cell lines (WIBR-iPS-SNCA$^{A53T\text{-}Corr}$-1 and -5) show only wild-type allele (G209 in 35 out of 35 sequences).
(D) Mutation analysis RT-PCR of α-synuclein transcript (± Tsp45I restriction digest) in indicated cell lines. (A53T mutation creates additional Tsp45I restriction site.) Expected fragment size after Tsp45I digest: wild-type transcript, 249/218/24/9 bp; A53T transcript, 249/185/33/24/9 bp (A53T and wild-type [wt]-derived restriction fragments are indicated by red arrows).
(E) Cytogenetic analysis of corrected PD patient-derived hiPSC line WIBR-iPS-SNCA$^{A53T\text{-}Corr}$-5 showing a normal karyotype.
(F) Immunofluorescence staining of WIBR-iPS-SNCA$^{A53T\text{-}Corr}$-5 line for the pluripotency markers OCT4, NANOG, SOX2, Tra-1-60, Tra-1-81, and SSEA4.
(G) Hematoxylin and eosin staining of teratoma sections generated from WIBR-iPS-SNCA$^{A53T\text{-}Corr}$-5 cells.
(H) Immunofluorescence staining of neuronal cultures derived from WIBR-IPS-SNCA$^{A53T\text{-}Corr}$-5 cells 10 days after induction of differentiation for neuron-specific class III β-tubulin (TUJ1; green) and the dopaminergic neuron-specific marker tyrosine hydroxylase (TH; red).

Dawson, T.M., Ko, H.S., and Dawson, V.L. (2010). Genetic animal models of Parkinson's disease. Neuron *66*, 646–661.

Dimos, J.T., Rodolfa, K.T., Niakan, K.K., Weisenthal, L.M., Mitsumoto, H., Chung, W., Croft, G.F., Saphier, G., Leibel, R., Goland, R., et al. (2008). Induced pluripotent stem cells generated from patients with ALS can be differentiated into motor neurons. Science *321*, 1218–1221.

Doyon, Y., McCammon, J.M., Miller, J.C., Faraji, F., Ngo, C., Katibah, G.E., Amora, R., Hocking, T.D., Zhang, L., Rebar, E.J., et al. (2008). Heritable targeted gene disruption in zebrafish using designed zinc-finger nucleases. Nat. Biotechnol. *26*, 702–708.

Doyon, Y., Vo, T.D., Mendel, M.C., Greenberg, S.G., Wang, J., Xia, D.F., Miller, J.C., Urnov, F.D., Gregory, P.D., and Holmes, M.C. (2011). Enhancing zinc-finger-nuclease activity with improved obligate heterodimeric architectures. Nat. Methods *8*, 74–79.

Ebert, A.D., Yu, J., Rose, F.F., Jr., Mattis, V.B., Lorson, C.L., Thomson, J.A., and Svendsen, C.N. (2009). Induced pluripotent stem cells from a spinal muscular atrophy patient. Nature *457*, 277–280.

Elliott, B., Richardson, C., Winderbaum, J., Nickoloff, J.A., and Jasin, M. (1998). Gene conversion tracts from double-strand break repair in mammalian cells. Mol. Cell. Biol. *18*, 93–101.

Golbe, L.I., Di Iorio, G., Sanges, G., Lazzarini, A.M., La Sala, S., Bonavita, V., and Duvoisin, R.C. (1996). Clinical genetic analysis of Parkinson's disease in the Contursi kindred. Ann. Neurol. *40*, 767–775.

Goldberg, A.D., Banaszynski, L.A., Noh, K.M., Lewis, P.W., Elsaesser, S.J., Stadler, S., Dewell, S., Law, M., Guo, X., Li, X., et al. (2010). Distinct factors control histone variant H3.3 localization at specific genomic regions. Cell *140*, 678–691.

Gore, A., Li, Z., Fung, H.L., Young, J.E., Agarwal, S., Antosiewicz-Bourget, J., Canto, I., Giorgetti, A., Israel, M.A., Kiskinis, E., et al. (2011). Somatic coding mutations in human induced pluripotent stem cells. Nature *471*, 63–67.

Hanna, J., Wernig, M., Markoulaki, S., Sun, C.W., Meissner, A., Cassady, J.P., Beard, C., Brambrink, T., Wu, L.C., Townes, T.M., and Jaenisch, R. (2007). Treatment of sickle cell anemia mouse model with iPS cells generated from autologous skin. Science *318*, 1920–1923.

Hockemeyer, D., Soldner, F., Cook, E.G., Gao, Q., Mitalipova, M., and Jaenisch, R. (2008). A drug-inducible system for direct reprogramming of human somatic cells to pluripotency. Cell Stem Cell *3*, 346–353.

Hockemeyer, D., Soldner, F., Beard, C., Gao, Q., Mitalipova, M., DeKelver, R.C., Katibah, G.E., Amora, R., Boydston, E.A., Zeitler, B., et al. (2009). Efficient targeting of expressed and silent genes in human ESCs and iPSCs using zinc-finger nucleases. Nat. Biotechnol. *27*, 851–857.

Hockemeyer, D., Wang, H., Kiani, S., Lai, C.S., Gao, Q., Cassady, J.P., Cost, G.J., Zhang, L., Santiago, Y., Miller, J.C., et al. (2011). Genetic engineering of human ES and iPS cells using TALE nucleases. Nat. Biotechnol. 10.1038/nbt.1927.

Hussein, S.M., Batada, N.N., Vuoristo, S., Ching, R.W., Autio, R., Närvä, E., Ng, S., Sourour, M., Hämäläinen, R., Olsson, C., et al. (2011). Copy number variation and selection during reprogramming to pluripotency. Nature *471*, 58–62.

Itzhaki, I., Maizels, L., Huber, I., Zwi-Dantsis, L., Caspi, O., Winterstern, A., Feldman, O., Gepstein, A., Arbel, G., Hammerman, H., et al. (2011). Modelling the long QT syndrome with induced pluripotent stem cells. Nature *471*, 225–229.

Laurent, L.C., Ulitsky, I., Slavin, I., Tran, H., Schork, A., Morey, R., Lynch, C., Harness, J.V., Lee, S., Barrero, M.J., et al. (2011). Dynamic changes in the copy number of pluripotency and cell proliferation genes in human ESCs and iPSCs during reprogramming and time in culture. Cell Stem Cell *8*, 106–118.

Lee, G., Papapetrou, E.P., Kim, H., Chambers, S.M., Tomishima, M.J., Fasano, C.A., Ganat, Y.M., Menon, J., Shimizu, F., Viale, A., et al. (2009). Modelling pathogenesis and treatment of familial dysautonomia using patient-specific iPSCs. Nature *461*, 402–406.

Lees, A.J., Hardy, J., and Revesz, T. (2009). Parkinson's disease. Lancet *373*, 2055–2066.

Lengner, C.J., Gimelbrant, A.A., Erwin, J.A., Cheng, A.W., Guenther, M.G., Welstead, G.G., Alagappan, R., Frampton, G.M., Xu, P., Muffat, J., et al. (2010). Derivation of pre-X inactivation human embryonic stem cells under physiological oxygen concentrations. Cell *141*, 872–883.

Marchetto, M.C.N., Carromeu, C., Acab, A., Yu, D., Yeo, G.W., Mu, Y., Chen, G., Gage, F.H., and Muotri, A.R. (2010). A model for neural development and treatment of Rett syndrome using human induced pluripotent stem cells. Cell *143*, 527–539.

Miller, J.C., Holmes, M.C., Wang, J., Guschin, D.Y., Lee, Y.-L., Rupniewski, I., Beausejour, C.M., Waite, A.J., Wang, N.S., Kim, K.A., et al. (2007). An improved zinc-finger nuclease architecture for highly specific genome editing. Nat. Biotechnol. *25*, 778–785.

Montgomery, S.B., Sammeth, M., Gutierrez-Arcelus, M., Lach, R.P., Ingle, C., Nisbett, J., Guigo, R., and Dermitzakis, E.T. (2010). Transcriptome genetics using second generation sequencing in a Caucasian population. Nature *464*, 773–777.

Närvä, E., Autio, R., Rahkonen, N., Kong, L., Harrison, N., Kitsberg, D., Borghese, L., Itskovitz-Eldor, J., Rasool, O., Dvorak, P., et al. (2010). High-resolution DNA analysis of human embryonic stem cell lines reveals culture-induced copy number changes and loss of heterozygosity. Nat. Biotechnol. *28*, 371–377.

Park, I.H., Arora, N., Huo, H., Maherali, N., Ahfeldt, T., Shimamura, A., Lensch, M.W., Cowan, C., Hochedlinger, K., and Daley, G.Q. (2008). Disease-specific induced pluripotent stem cells. Cell *134*, 877–886.

Perez, E.E., Wang, J., Miller, J.C., Jouvenot, Y., Kim, K.A., Liu, O., Wang, N., Lee, G., Bartsevich, V.V., Lee, Y.-L., et al. (2008). Establishment of HIV-1 resistance in CD4+ T cells by genome editing using zinc-finger nucleases. Nat. Biotechnol. *26*, 808–816.

Pickrell, J.K., Marioni, J.C., Pai, A.A., Degner, J.F., Engelhardt, B.E., Nkadori, E., Veyrieras, J.-B., Stephens, M., Gilad, Y., and Pritchard, J.K. (2010). Understanding mechanisms underlying human gene expression variation with RNA sequencing. Nature *464*, 768–772.

Polymeropoulos, M.H., Lavedan, C., Leroy, E., Ide, S.E., Dehejia, A., Dutra, A., Pike, B., Root, H., Rubenstein, J., Boyer, R., et al. (1997). Mutation in the alpha-synuclein gene identified in families with Parkinson's disease. Science *276*, 2045–2047.

Radecke, F., Peter, I., Radecke, S., Gellhaus, K., Schwarz, K., and Cathomen, T. (2006). Targeted chromosomal gene modification in human cells by single-stranded oligodeoxynucleotides in the presence of a DNA double-strand break. Mol. Ther. *14*, 798–808.

Radecke, S., Radecke, F., Cathomen, T., and Schwarz, K. (2010). Zinc-finger nuclease-induced gene repair with oligodeoxynucleotides: wanted and unwanted target locus modifications. Mol. Ther. *18*, 743–753.

Rashid, S.T., Corbineau, S., Hannan, N., Marciniak, S.J., Miranda, E., Alexander, G., Huang-Doran, I., Griffin, J., Ahrlund-Richter, L., Skepper, J., et al. (2010). Modeling inherited metabolic disorders of the liver using human induced pluripotent stem cells. J. Clin. Invest. *120*, 3127–3136.

Richardson, C., and Jasin, M. (2000). Coupled homologous and nonhomologous repair of a double-strand break preserves genomic integrity in mammalian cells. Mol. Cell. Biol. *20*, 9068–9075.

Saha, K., and Jaenisch, R. (2009). Technical challenges in using human induced pluripotent stem cells to model disease. Cell Stem Cell *5*, 584–595.

Schulz, J.B. (2008). Update on the pathogenesis of Parkinson's disease. J. Neurol. *255* (*Suppl 5*), 3–7.

Soldner, F., Hockemeyer, D., Beard, C., Gao, Q., Bell, G.W., Cook, E.G., Hargus, G., Blak, A., Cooper, O., Mitalipova, M., et al. (2009). Parkinson's disease patient-derived induced pluripotent stem cells free of viral reprogramming factors. Cell *136*, 964–977.

Summers, K.M. (1996). Relationship between genotype and phenotype in monogenic diseases: relevance to polygenic diseases. Hum. Mutat. *7*, 283–293.

Takahashi, K., Tanabe, K., Ohnuki, M., Narita, M., Ichisaka, T., Tomoda, K., and Yamanaka, S. (2007). Induction of pluripotent stem cells from adult human fibroblasts by defined factors. Cell *131*, 861–872.

Urnov, F.D., Miller, J.C., Lee, Y.-L., Beausejour, C.M., Rock, J.M., Augustus, S., Jamieson, A.C., Porteus, M.H., Gregory, P.D., and Holmes, M.C. (2005).

Highly efficient endogenous human gene correction using designed zinc-finger nucleases. Nature *435*, 646–651.

Urnov, F.D., Rebar, E.J., Holmes, M.C., Zhang, H.S., and Gregory, P.D. (2010). Genome editing with engineered zinc finger nucleases. Nat. Rev. Genet. *11*, 636–646.

Vogel, G. (2010). Stem cells. Diseases in a dish take off. Science *330*, 1172–1173.

Yu, J., Vodyanik, M.A., Smuga-Otto, K., Antosiewicz-Bourget, J., Frane, J.L., Tian, S., Nie, J., Jonsdottir, G.A., Ruotti, V., Stewart, R., et al. (2007). Induced pluripotent stem cell lines derived from human somatic cells. Science *318*, 1917–1920.

Zarranz, J.J., Alegre, J., Gómez-Esteban, J.C., Lezcano, E., Ros, R., Ampuero, I., Vidal, L., Hoenicka, J., Rodriguez, O., Atarés, B., et al. (2004). The new mutation, E46K, of alpha-synuclein causes Parkinson and Lewy body dementia. Ann. Neurol. *55*, 164–173.

Zou, J., Maeder, M.L., Mali, P., Pruett-Miller, S.M., Thibodeau-Beganny, S., Chou, B.-K., Chen, G., Ye, Z., Park, I.-H., Daley, G.Q., et al. (2009). Gene targeting of a disease-related gene in human induced pluripotent stem and embryonic stem cells. Cell Stem Cell *5*, 97–110.